Soft Matter

Accepted Manuscript

ROYAL SOCIETY OF CHEMISTRY

www.rsc.org/softmatter

Cite this: DOI: 10.1039/c0xx00000x

www.rsc.org/xxxxxx

PAPER

Thermal phase transition behaviours of the blue phase of bent-core nematogen and chiral dopant mixtures under different boundary conditions

Min-Jun Gim,[a] Gohyun Han,[a] Suk-Won Choi,*[b] and Dong Ki Yoon*[a]

Received (in XXX, XXX) XthXXXXXXXXX 20XX, Accepted Xth XXXXXXXXX 20XX
DOI: 10.1039/b000000x

We have investigated dramatic changes in the thermal phase transition of a liquid-crystalline (LC) blue phase (BP) consisting of bent-core nematogen and chiral dopant in various boundary conditions during cooling from the isotropic phase. Blue phase III, which has arbitrary morphological characteristics, between two glass plates goes to blue phase I, which has a body-centred cubic structure, when the sample is placed on the glass as a droplet form. These two distinctive phase transition behaviours were directly observed by polarized optical microscopy as well as selective reflection spectroscopy, in which the phase transition between BPs started from the air/LC interface. We determined that this transition resulted from the ordered double-twisted cylinders near the air-boundary by confocal laser-scanning microscopy.

Introduction

Chiral liquid crystal (LC) phases such as the chiral nematic phase (N*) and blue phases (BPs) can be simply created with chiral additives in nematic LC materials.[1] In particular, the nano-scale double-twisted cylinder (DTC), a building block of BPs, can be produced under a very strong helical twisting power using a high concentration of chiral agents to minimize the local free energy, revealing structures that are more frustrated structures than N*. Then, DTCs are spontaneously organized into three BP forms depending on the packing sequences during cooling from the isotropic phase: the multi-colour BP I, BP II, and the misty blue BP III. The BP III form has randomly ordered DTCs, showing amorphous optical properties,[2] while BP I and BP II have body-centred cubic and simple cubic structures, respectively, revealing colourful morphologies under cross-polarizers.[3] The unique periodic structures of cubic BPs generate photonic band gaps in the visible wavelength range, where light corresponding to a range of forbidden frequencies cannot propagate through self-assembled photonic crystals composed of DTCs.[4]

The BPs are highly attractive for opto-electronic applications such as displays, optical modulators, and lasing systems due to their intriguing structural and optical properties. For example, in lasing systems based on LC materials, BPs have many advantages compared to conventional methods. First, for photonic crystals, self-organized cubic BPs do not need any additional complex fabrication processes. Second, periodic photonic crystals provide flexible photonic band gaps, resulting from variations in the unit cell dimensions of BPs.[4] Third, a laser system based on BPs exhibits a lower excitation threshold energy than one-dimensional photonic crystals of conventional N*.[5,6] Finally, the photonic band gap of cubic BPs can be tuned by applying by external stimuli such as temperature gradients,[7,8] electric and magnetic fields,[9,10] and light.[11] However, cubic BPs between two substrates, the surface of which are untreated, exhibit multi-platelet domains showing multi-colours originating from randomly oriented lattice planes. On the contrary, uniformly oriented lattices can be induced by surface treatment of substrates.[12,13,14] This is caused by a strong anchoring effect induced from the surface, leading to a decrease in the colour tunability range. This small colour tunability range has been a critical limit for the practical uses.

To achieve a broad colour tunability range in large mono-domains possessing uniformly oriented lattices in this study, we use anisotropic surface boundary conditions, in which the LC molecules exhibit planar anchoring on the bottom substrate and homeotropic anchoring near LC/air boundary.[15,16] We use depolarized transmitted light microscopy (DTLM), depolarized reflected light microscopy (DRLM), and confocal laser-scanning microscopy (CLSM) to characterize BP droplets prepared on the planar-aligned substrate on cooling from isotropic phase. Selective reflection spectroscopy was used to confirm the BP I phase compared to BP III.

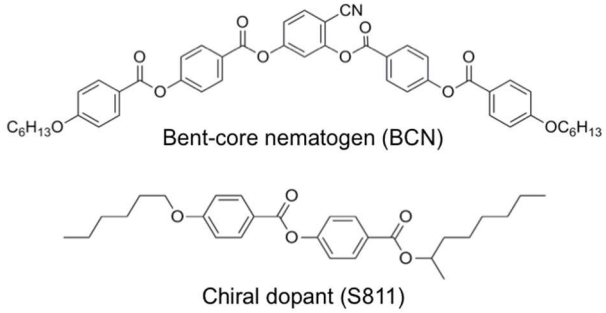

Fig. 1 Molecular structures of bent-core nematogen and chiral dopant used for the BP mixture.

Experimental

Sample preparation

A BP mixture consists of 21 wt %-chiral dopant (S811, Merck) and 79 wt%-bent-core nematogen[17]. The bent-core nematogen has the following phase sequence on cooling: isotropic phase − (140°C) − nematic phase − (105°C) − crystalline phase. The chemical structures of chiral dopant and ben-core molecules used here are depicted in Figure 1. To investigate the influence of the surface boundary conditions on BPs, we prepared two different samples: a sandwiched cell between glasses and a droplet on a silicon wafer. For the sandwiched cell, the mixture was injected into a sandwich cell fabricated with two glass substrates at isotropic temperatures, and the cell gap was fixed with 50-μm film spacers. For the droplet sample, the mixture was dropped on a silicon wafer substrate. All substrates were washed with organic solvents and treated with O_2 plasma before the mixture was loaded to induce planar alignment of molecules on the substrate.

Optical characterization

The optical textures were characterized by DTLM and DRLM during the phase transition. All phase transition experiments were started after the samples were maintained at 115°C for 20 minutes on the heating stage (LINKAM LTS350) using a temperature controller (LINKAM TMS94) for thermal stabilization. Then, the samples were slowly cooled from 115°C to 80°C at a rate of 0.05°C /min to observe the phase transitions from isotropic to N* via BP III and BP I. The selective reflection spectra were collected using a USB-2000+ spectrometer (Ocean Optics). Moreover, three-dimensionally captured images of the textures were taken by CLSM (C2 Plus, Nikon) with a laser source at 488 nm (Coherent).[18] The images were recorded by a cooled charge-coupled device (CCD) colour camera (DS-Ri1).

Results and Discussions

Generally, BP III shows the amorphous misty blue texture without any domain-like structures, while cubic BPs show platelet textures, which consist of differently oriented domains. According to previous studies, a mixture of biaxial molecules (such as “bent-core” or “T-shape” molecules) and chiral dopants

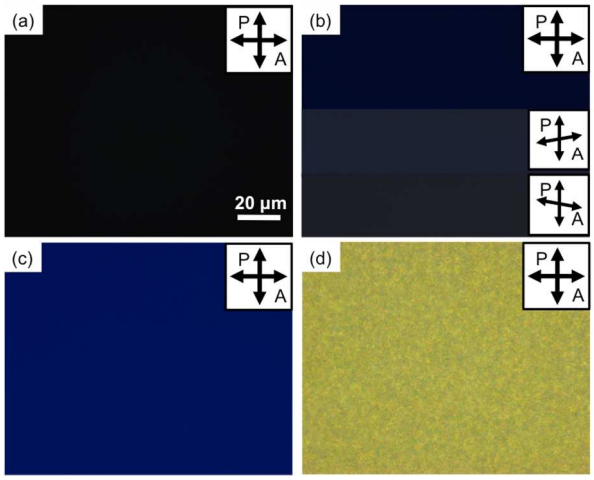

Fig. 2 The DTLM images of the sandwich cell during the cooling: (a) isotropic phase at 95°C, (b) BP III at 92.0°C (c) BP III at 90°C, (d) N* at 88.0°C. Depending on the rotation of the analyzer, BP III shows different brightness of textures. In N*, the focal conic textures emerge and exhibit bright morphologies compared to BP III.

tends to have only one phase, BP III, while BPs based on classic rod-type molecules can have BP III as well as cubic BPs during cooling from the isotropic phase.[19,20,21,22,23] This is resulted from the biaxial shape of molecules. The helical twisting power induced by chiral dopants primarily acts on the long axis of a molecule, while the dipole moment between the short axes coincides in a biaxial molecule. This coupling between chirality and biaxiality presents much a larger twisting power than that found in the convectional rod-type molecular system.[24,25,26] Here, we prepared a BP mixture with this biaxial molecular system with chiral dopants (Figure 1).

During the thermal transition, morphological changes were observed over the majority of the sample; examples of the morphological changes are shown in Figure 2. The BP III phase, which occurs over a very short (~4°C) temperature range, appears between the isotropic phase and N* during the cooling process, which is quite normal for BPs with biaxial molecules. During the cooling process, platelet textures, which are typical textures of cubic BPs, did not appear, and the only uniform misty blue texture was exhibited in a large area over hundreds of microns (Figure 2b). In order to examine the existence of BP III, the analyzer was slightly rotated in clockwise and counter-clockwise

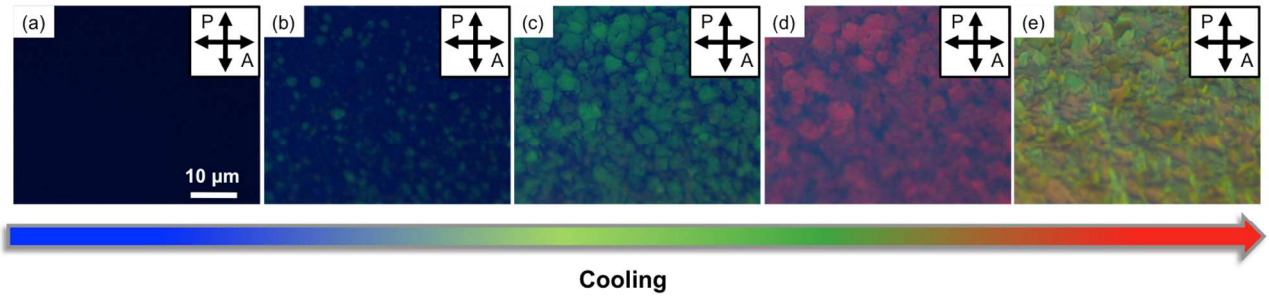

Fig. 3 The DRLM images of the droplet on the silicon wafer treated with O_2 plasma during the cooling. (a) Amorphous misty blue BP III appeared at 93°C, (b) platelet textures representative of cubic BP I nucleated at 92.0°C, and (c) the platelet textures covered the entire area at 91.2°C. (d) The BP I exhibited a red shift at 90.2°C, and (e) focal conic domains of N* appeared from cubic BP I without deformation of the domain structures at 89.5°C.

directions, showing different brightness due to its strong optical activity.[22] On the other hand, the isotropic phase exhibits no optical signal (Figure 2a). Therefore, the optical textures support the existence of BP III in our sample as reported previously. The phase sequence in sandwich cell was observed at different wt % of chiral dopant. Only one BP III emerged between isotropic and N* at overall BP mixtures. (ESI, Figure S1†).

On the other hand, DRLM images of the droplet sample of the mixture on a silicon wafer revealed morphologies that were very different from those observed in the sandwich cell. In particular, morphological changes of amorphous misty blue to colourful platelet textures were observed over a large area as the sample cooled (Figure 3). During the thermal transition, first the amorphous misty blue texture of BP III appears at 93°C as shown in the sandwich cell (Figure 3a). The platelet textures then formed, and the nucleation and growth of the platelet structures in BPs displayed the following typical characteristics on cooling from BP III. (1) The green platelet textures with small blue domains nucleate (Figure 3b), covering the entire view field in DTLM measurements at 91.2°C (Figure 3c). Here, green platelet textures are result of the appearance of periodic structures, which reflect specific wavelengths when it satisfies Bragg reflection condition. (2) Without many morphological changes, a red shift gradually occurs at 90.2°C (Figure 3d), which provides strong evidence that the emerged cubic phase is the BP I phase because BP II normally exhibits a blue shift as the temperature decreases.[7,9] (3) Then, the focal conic textures representing N* emerge slightly below the temperature of BP I (89.5°C) (Figure 3e). (4) Finally, crystal structures appear at 87°C. The overall phase transition order for the droplet sample of the mixture is isotropic – BP III – BP I – N* – Crystal, which is quite different from the sandwich sample that has isotropic – BP III – N* – Crystal transition sequences. Table 1 shows the phase transition temperatures determined from polarized light microscopy results for both the mixture in the sandwiched cell and on silicon wafer.

The observation of selective reflection spectra as a function of temperature can show more qualitative and quantitative phase transition behaviour than the imaging technique. In order to study the optical properties of the droplet sample, we investigated the selective spectra at each phase (BP III, BP I, N*) during the phase transition (Figure 4a). At BP III, a broad range of reflectance from 473 nm to 486 nm could be observed with weak intensity at 92.0°C. On the other hand, BP I shows a relatively sharp and strong reflection peak in which cubic lattices satisfy Bragg's reflection condition. The BP III peak at ~486 nm started to disappear during the BP III – BP I transition where the BP I peak gradually increased (Figure 4b). During the phase transition, the discontinuous reflection wavelength gap in the BP III – BP I transition was about 30 nm, which can explain the sudden change of colours in DRLM measurements (Figures 3a and b). Finally, the reflection wavelength of BP I showed a red shift with decreasing temperature, corresponding to DRLM images (Figures 3b and c).

The unusual phase transition behaviour of the blue phase of bent-core nematogen and chiral dopant mixture results from the simple anisotropic boundary condition of the planar-aligned bottom-substrate and the homeotropic-aligned LC/air interface. The relatively weak surface or anchoring energy of LC/air compared to LC/LC and LC/silicon substrate triggers the formation of perpendicularly aligned LC molecules, leading to highly ordered DTCs that will pack to form cubic BP I through arbitrary orientated BP III. Kitzerow et al. describe a similar behaviour in the unique electrical field induced BP phase named "BPE," which mostly coexists with BP III.[2] They measured reflection spectra as a function of electric field to see the transition from BP III to BPE. In a strong electric field, the well-ordered BP III phase was found near substrates, resulting in a sharper reflection peak, corresponding to the higher periodicity of DTCs. Furthermore, Bouligand et al. directly observed a topological pattern in a droplet of BPs on glass,[27] which exhibited herring-bone-type N* textures during the phase transition from BP to N*. These previous works provide insight into the influence of the air boundary on BPs droplet in our system.

In order to compare different morphologies of our system in the droplet on the substrate as well as near air boundary, a CLSM experiment was performed at the transition point between BP III

Table. 1 Thermal transition of BPs with different boundary conditions. The mixture was injected into a sandwich cell of two glass plates and dropped on a silicon wafer.

Sample condition	Phase transition temperature (°C)									
	Crystal		N*		BPI		BPIII		Isotropic	
Sandwich cell	•	88.0	•	88.2	×	-	•	92.7	•	
Droplet	•	87.0	•	89.5	•	92.0	•	93.0	•	

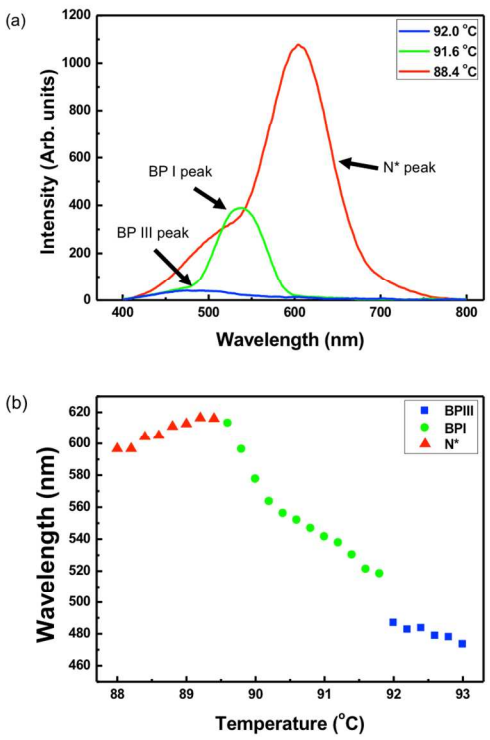

Fig. 4 (a) Reflection spectra of the droplet on a silicon wafer in different phases; blue line is BP III, green line is BP I and red line is N*. (b) Selective reflection wavelength of the droplet as a function of temperature.

and BP I. Generally, fluorescent dyes should be used to observe the fluorescent signal from the target specimen for the CLSM study, but cubic BPs that exhibit Bragg reflection can be imaged without adding fluorescent dyes.[18] Figure 5a shows the perspective view of the CLSM image of the droplet on a silicon wafer at 91.6°C where BP I generated from BP III. The cubic lattices of BP I nucleated from the air/LC interface, growing toward the silicon wafer substrate. The BPs coexisting at the transition point in Figure 3b are now separately imaged with the CLSM technique, and they can be distinguished by the reflected light intensity. In this case, BP I exhibits strong reflected light intensity from the platelet domains due to the well-ordered cubic lattices, while BP III shows a weak reflected light intensity on account of the disordered DTCs. The vertical cross sections of a three-dimensional CLSM image clearly show the two-separated BPs (Figure 5b). The top of the droplet, which shows a strong intensity, is BP I, while the bottom area reveals weak intensity, representing BP III. Moreover, BP I can be found in the xy in-plane image (Figure 5c), covering the whole sample area 44 μm from the bottom of the substrate. On the other hand, a totally dark image, representing BP III, was observed at 21 μm in the same intensity offset as that in the BP I case (Figure 5d). Based on the CLSM study, the phase transition from BP III to BP I starts from air/LC interface of the droplet, which indicates that the homeotropic alignment of LC molecules induced from the air boundary generates the highly ordered cubic BP I.

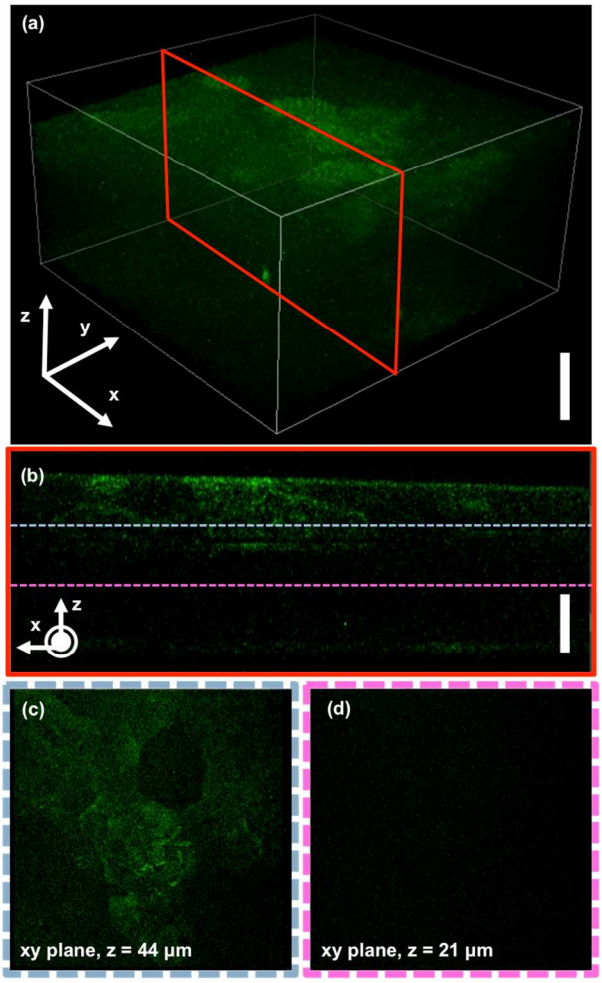

Fig. 5 The CLSM images of the droplet on a silicon wafer at the BP III – BP I transition temperature. (a) A perspective view of the CLSM image at 91.6°C. (b) Vertical cross sections of the x-z plane of the droplet. The white bar corresponds to 20 μm. The in-plane (x-y) images at (c) 44 μm and (d) 21 μm from bottom.

The CLSM study clearly shows that BP I emerged via BP III under the anisotropic boundary condition of air and a planar-aligned silicon substrate upon cooling. It is generally well known that the helical twisting power of helical structures such as N* and BPs decreases on cooling,[8] and a light-tuning method has been used to control this behaviour.[11] In high temperature BP III, the helical twisting power is so strong that the LC molecules in DTCs should be highly twisted, resulting in disordered DTCs to form BP III regardless of the boundary conditions. However, in low temperature BP III or high temperature BP I, the perpendicularly aligned LC molecules near LC/air interface could perturb the helical twisting power of DTCs or BPs. Like the BPE case,[2] this small external stimulus could move DTCs from the air/LC boundary and organize them into relatively high-ordered structures such as BP I. This initial or nucleating reaction of BP I could extend to the whole sample area, and we could observe BP I with microscopy.

Conclusions

We studied the correlation between the phase transition behaviours of BPs and different boundary conditions in this work. Unlike the sandwiched cell where the BP mixture exhibited only BP III, the droplet sample showed BP III as well as BP I on cooling from the isotropic phase. Due to the thermal gradient resulting from the heating stage placed under the sample opened to air, the nucleation of DTCs starts from the LC/air interface, forming highly ordered cubic BP I via randomly ordered BP III of DTCs. The chiral diffusion by the thermal gradient can be raised, but we ignore the phenomenon, since BP I didn't appear during cooling even low chirality in sandwich cell (Figure S1). And the BP I always emerged in a droplet sample where homeotropic anchoring exhibits near LC/air interface. This results support that the emergence of BP I is due to an influence of homeotropic anchoring from air, not chirality diffusion. Moreover, the BP I exhibited uniform mono-domains with a single reflection colour, showing a red-colour shift as temperature decreased. This resultant phase behaviour can be used for developing a tunable LC BP laser that has unique properties of wide colour shift, large area, high efficiency, and low excitation threshold energy.

Acknowledgements

The first two authors contributed equally to this work. This was supported by Basic Science Research Program (2012R1A1A1002486 and 2012R1A2A2A06046931) through National Research Foundation (NRF) grant funded by the MSIP, Korea.

Notes and references

[a] *Graduate School of Nanoscience and Technology and Center for Nature-inspired Technology in KAIST Institute for the NanoCentury,*

KAIST, Daejeon, 305-701, Republic of Korea. Fax: +82 42 350 1110; Tel: +82 42 350 1156; E-mail: nandk@kaist.ac.kr

[b] *Department of Advanced Materials Engineering for Information & Electronics, Kyung Hee University, Yongin, Gyeonggi-do, 446-701, Republic of Korea.*

† Electronic Supplementary Information (ESI) available: [details of any supplementary information available should be included here]. See DOI: 10.1039/b000000x/

‡ Footnotes should appear here. These might include comments relevant to but not central to the matter under discussion, limited experimental and spectral data, and crystallographic data.

1. P. P. Crooker, in *Chirality in Liquid Crystals*, ed. H.-S. Kitzerow and C. Bahr, Springer, New York, 2001, pp. 186-222.
2. H.-S. Kitzerow, P. P. Crooker, and G. Heppke, *Phys. Rev. Lett.*, 1991, **67**, 2151–2154.
3. D. C. Wright and N. D. Mermin, *Rev. Mod. Phys.*, 1989, **61**, 385–432.
4. W. Y. Cao, A. Munoz, P. Palffy-Muhoray, B. Taheri, *Nat. Mater.* 2002, **1**, 111-113.
5. M. H. Song, B. Park, K. Shin, T. Ohta, Y. Tsunoda, H. Hoshi, Y. Takanishi, K. Ishikawa, J. Watanabe, S. Nishimura, T. Toyooka, Z. Zhu, T. M. Swager, and H. Takezoe, *Adv. Mater.* 2004, **16**, 779-783.
6. H. J. Coles and S. M. Morris, Nat. Photon. 2010, **4**, 676-685
7. H. Choi, H. Higuchi, H. Kikuchi, *Appl. Phys. Lett.* 2011, **98**, 131906-1-3.
8. S.-T. Hur, B. R. Lee, M.-J. Gim, K.-W. Park, M. H. Song, and S.-W. Choi, *Adv. Mater.* 2013, **25**, 3002–3006.
9. H. J. Coles and M. N. Pivnenko, *Nature* 2005, **436**, 997-1000.
10. S. Shibayama, H. Higuchi, Y. Okumura, and H. Kikuchi, *Adv. Funct. Mater.* 2013, **23**, 2387-2396.
11. T.-H. Lin, Y. Li, C.-T. Wang, H.-C. Jau, C.-W. Chen, C.-C. Li, H. K. Bisoyi, T. J. Bunning, and Q. Li, *Adv. Mater.* 2013, **25**, 5050-5054.
12. C. T. Wang, H.-C. Jau, and T. H. Lin, *Opt. Mater.*, 2011, **34**, 248–250.
13. H. Choi, H. Higuchi, and H. Kikuchi, *Soft Matter*, 2011, **7**, 4252–4256.
14. J. Yan, S. T. Wu, K.-L. Cheng, and J.-W. Shiu, *Appl. Phys. Lett.*, 2013, **102**, 081102-1-5.
15. H. Kim, Y. Yi, D. Chen, E. Körblova, D. M. Walba, N. A. Clark, and D. K. Yoon, *Soft Matter*, 2013, **9**, 2793–2797.
16. H. Kim, S. Lee, T. J. Shin, Y. J. Cha, E. Körblova, D. M. Walba, N. A. Clark, S. B. Lee, and D. K. Yoon, *Soft Matter*, 2013, **9**, 6185–6191.
17. L. Kovalenko, M. W. Schröder, R. Amaranatha Reddy, S. Diele, G. Pelzl, and W. Weissflog, *Liq. Cryst.*, 2005, **32**, 857–865.
18. K. Higashiguchi, K. Yasui, and H. Kikuchi, *J. Am. Chem. Soc.*, 2008, **130**, 6326–6327.

`Mieczkowski, A. Jakli, K. Ishikawa, and H. Takezoe, *J. Mater. Chem.*, 2011, **21**, 2855–2857.

20. A. Yoshizawa, M. Sato, and J. Rokunohe, *J. Mater. Chem.*, 2005, **15**, 3285–3290.
21. M. Sato and A. Yoshizawa, *Adv. Mater.*, 2007, **19**, 4145–4148.
22. A. Yoshizawa, *J. Info. Display*, 2008, **16**, 1189–1194.
23. S. Taushanoff, K. Van Le, J. Williams, R. J. Twieg, B. K. Sadashiva, H. Takezoe, and A. Jakli, *J. Mater. Chem.*, 2010, **20**, 5893–5898.
24. Z. Zheng, D. Shen, and P. Huang, *New J. of Phys*, 2010, **12,** 113018-1-10.
25. M. Marik, A. Mukherjee, D. Jana, and A. Yoshizawa, *Phys. Rev. E*, 2013 **88,** 012502-1-7.
26. M. Tanaka and A. Yoshizawa, *J. Mater. Chem. C*, 2013, **1**, 315–320.
27. Y. Bouligand, S. T. Lagerwall, and B. Stebler, *Comptes Rendus Chimie*, 2008, **11,** 212-220.